Received: 19 May 2016 | Revised: 31 January 2017 | Accepted: 20 April 2017

DOI: 10.1002/qre.2167

RESEARCH ARTICLE

WILEY

Statistical process monitoring via image data using wavelets

Mehdi Koosha[1] | Rassoul Noorossana[1] | Fadel Megahed[2]

[1] Industrial Engineering Department, Iran University of Science and Technology, Tehran, Tehran Province, Iran

[2] Department of Information Systems and Analytics, Miami University, Oxford, Ohio, USA

Correspondence
Rassoul Noorossana, Industrial Engineering Department, Iran University of Science and Technology, Tehran, Tehran Province, Iran.
Email: rassoul@iust.ac.ir

Abstract

Image data plays an important role in manufacturing and service industries because each image can provide a huge set of data points in just few seconds with relatively low cost. Enhancement of machine vision systems during the time has led to higher quality images, and the use of statistical methods can help to analyze the data extracted from such images efficiently. It is not efficient from time and cost point of views to use every single pixel in an image to monitor a process or product performance effectively. In recent years, some methods are proposed to deal with image data. These methods are mainly applied for separation of nonconforming items from conforming ones, and they are rarely applied to monitor process capability or performance. In this paper, a nonparametric regression method using wavelet basis function is developed to extract features from gray scale image data. The extracted features are monitored over time to detect process out-of-control conditions using a generalized likelihood ratio control chart. The proposed approach can also be applied to find change point and fault location simultaneously. Several numerical examples are used to evaluate performance of the proposed method. Results indicate suitable performance of the proposed method in detecting out-of-control conditions and providing precise diagnostic information. Results also illustrate suitable performance of our proposed method in comparison with a competitive approach.

KEYWORDS

change point, control chart, generalized likelihood ratio test, gray scale image, phase II methods, profile monitoring

1 | INTRODUCTION

Traditionally, quality characteristics are monitored using univariate or multivariate control charts. However, in certain applications, a relationship between a response variable and 1 or more explanatory variables that is referred to as profile can be used to monitor the performance of a product or process. In such a circumstance, process or product monitoring consists of estimating profile coefficients and using a control scheme to monitor them over time. Considering this functional relationship, profiles can be classified to different categories such as simple linear, multiple linear, spline, and logistic. Readers are referred to Noorossana et al[1] for more information about profile monitoring techniques.

In recent years, one of the most challenges faced by practitioners is how to deal with complicated-structured data in a statistical framework to evaluate process stability and capability to produce high quality products with low variation. One sort of complicated-structured data is image data that has an increasing application in real-life problems. Recently, noncontact image-based data-gathering techniques have gained an increasing attention among researchers. Using images for detection purposes and separating conforming products from nonconforming ones has been used in practice

for many years. Machine vision systems (MVSs) are widely used in industries because of their ability to provide information such as geometric features, surface defects, and surface finish. Because of the availability of MVS, image data are readily available in a short time at relatively low cost. An MVS is a computer system that uses 1 or more capture devices such as camera or X-ray device to extract data from image to perform a comprehensive analysis. It consists of a capturing step, an analysis step, a decision-making step using image analysis, and a system performance improvement step. Machine vision system has many advantages to human eye such as its capability to be used for monitoring high production-rate processes, performing multitasks on various products, and covering all range of electromagnetic spectrum. Moreover, the use of MVS is cheaper than human inspection. These advantages and its wide range of applications make MVS a suitable replacement for human inspection.

Defect detection techniques based on image data use textural features and search for significant deviations from the nominal value. Texture analysis techniques can be classified into 2 main categories of spatial domain and frequency domain. The most well-known methods for spatial domain texture analysis use gray level co-occurrence matrix and extract various features from that. Siew et al[2] and Latif- Amet et al[3] are examples for this type of texture analysis.

In frequency domain methods, textural features are extracted by applying frequency transforms such as Fourier, Gabor, or wavelet. Wavelet transform is the most popular method for feature extraction in recent years. Tico et al[4] applied wavelet transforms for finger-print recognition. Sari-Sarraf and Goddard[5] applied wavelet-based preprocessing for woven fabric defect detection. Ngan et al[6] proposed a method for patterned fabric defect detection based on wavelet transforms. Liu and MacGregor[7] proposed a wavelet-based method for defect detection in engineered stone countertops. They used Hoteling T^2 and squared prediction error control charts to detect defected products and defect location, respectively. Lin[8,9] proposed an automated visual inspection system based on wavelet characteristics to find defects in surface barrier layer. They applied multivariate statistics including Hoteling T^2, Mahalanobis distance D^2, and chi-square χ^2. Figure 1 shows the overlap rates between distributions of the defected and the normal texture under different methods (Lin[8]).

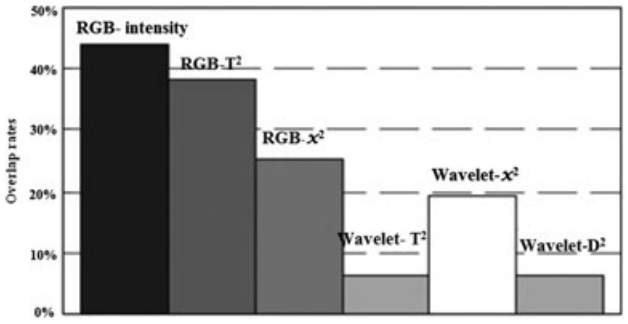

FIGURE 1 Overlap rates between distributions of the detected and normal textures under different methods (Lin[8])

Figure 1 illustrates that wavelet-based methods are superior to those methods directly applied to raw images in detecting defects (Lin[8]). Lin et al[10] applied principal component analysis on 2-dimensional (2D) wavelet characteristics for dimension reduction and used light-emitting diode (LED) as their case study. They used T^2 control chart to signal for water-spot defects on LED surface. Li and Tsai[11] used a wavelet-based method for defect detection in solar wafer images with inhomogeneous texture.

It is well known that statistical process control (SPC) is a powerful tool to prevent production of defects and nonconforming products. There exist 2 phases in SPC; phase I that deals with estimating process parameters to ensure process stability using historical data, and phase II pertains to signal any out-of-control condition or shifts in the process parameters. Researchers believe that control charts are the most featured tool of SPC. Control charts can be classified into 2 categories of univariate and multivariate charts. In univariate control charts, one is interested in monitoring changes in the parameter of an underlying univariate distribution over time. However, in multivariate control charts, one is interested in monitoring simultaneous changes in the parameter vector of an underlying multivariate distribution over time.

There are many applications in industries such as textile and LED panels where image data and univariate or multivariate control charts are considered to separate nonconforming items from the conforming ones. Several authors including Jiang and Jiang,[12] Lu and Tsai,[13] Tunák and Linka,[14]Armingol et al,[15] and Jiang et al[16] applied textural features in spatial domain for detecting the location or size of a fault using spatial control charts. A thorough literature review about applications of image data in control charting schemes is proposed by Megahed et al.[17]

It is very appealing to integrate SPC with image processing techniques to develop a control charting approach based on the collected image data. Through this combination, the procedure could use the benefits of SPC techniques and the information captured in an image simultaneously. Few researches have used image data in SPC framework. Megahed et al[18] proposed a spatiotemporal method that applied gray scale image data. In their proposed approach, image and its spatial domain features are used for SPC purposes.

This paper proposes a new wavelet-based method for SPC monitoring of gray scale image data. This method benefits from the suitable features of frequency domain. In the proposed method, after the preprocessing step, each image is decomposed into a number of 1-dimensional (1D) profiles and the method developed by Chicken[19] is used to monitor the resulted 1D profiles. We believe that integration

of feature extraction methods and SPC charts to monitor extracted frequency–based features such as wavelet coefficients can lead to considerable improvements in the performance evaluation metrics.

In the proposed method, we first apply wavelet transformation to extract the main features of the image to monitor them over time. Since a large number of extracted features is obtained from each image, we cannot simply use the traditional multivariate control charts to monitor process performance. The reason lies in the deteriorating property of traditional control charts when the number of quality characteristics increases. A generalized likelihood ratio (GLR) control chart is applied to confront this problem. This control chart can provide significant diagnostic information that helps practitioners to make proper decisions and restore the process to in-control condition. Table 1 shows a summarized review of the related papers and the position of the proposed method among other papers.

Numerous simulation studies are performed to evaluate the performance of the proposed method in detecting shifts and estimating fault location and change point. Moreover, we have compared our results with the ones achieved by Megahed et al[18] to confirm the performance of the proposed method. Their method also uses gray scale images, and it is appealing to consider their method as a competitive approach in this paper.

The remainder of this paper is organized as follows. Section 2 discusses nonparametric regression and wavelet transformation. Section 3 explains the proposed approach for statistical process monitoring using image data. Section 4 presents the results for the simulation studies, performance evaluation, and comparison with a competitive approach. A real case study in tile manufacturing industry is discussed in Section 5. Our concluding remarks are provided in the final section.

2 | DISCRETE WAVELET TRANSFORMATION AND MULTIRESOLUTION ANALYSIS

In parametric regression, shape of the relationship and the number of coefficients are predetermined and the objective is to estimate parameters to minimize a criterion such as mean squared error. In many real case problems, this function could be complicated and consists of many sharp changes. In these instances, nonparametric regression could be implemented as a powerful method for parameter estimation and variation explanation. In nonparametric regression, function does not have a predefined shape (Nikoo and Noorossana[20]) and the objective is to obtain a regression function with the least number of coefficients while having a good fit to the observations. Profiles derived from images usually have many sharp changes in many practical situations. Figures 2A,B shows a tile image and a profile derived from the first row of its intensity matrix, respectively.

For these sharp changes in the derived profiles, nonparametric methods should be used to obtain a regression model. It is assumed that the reader is not familiar with the concepts of nonparametric regression and wavelet transformation. So this section is devoted to a summarized introduction about these 2 concepts.

A general regression model can be represented as follows.

$$Y_i = f(x_i) + \varepsilon_i, \tag{1}$$

where i is a counter for profiles, Y_i is the independent variable,

TABLE 1 Position of the proposed method among other researches

	Frequency Domain	Fault Location	Fault Size	Change Point	Phase II Evaluation	Control Chart
Jiang and Jiang[12]	-	✓	✓	-	-	I/MR
Armingol et al.[15]	-	✓	✓	-	-	I/MR
Jiang et al.[16]	-	✓	✓	-	-	EWMA
Lu and Tsai[13]	-	✓	✓	-	-	X-bar
Tunák and Linka[14]	-	✓	✓	-	-	T^2
Ngan et al.[6]	✓	✓	✓	-	-	-
Liu and MacGregor[7]	✓	✓	✓	-	-	T^2 + SPE
Lin[8]	✓	✓	✓	-	-	$T^2/D^2/\chi^2$
Lin et al.[10]	✓	✓	✓	-	-	T^2
Li and Tsai[11]	✓	✓	✓	-	-	-
Megahed et al.[18]	-	✓	✓	✓	✓	GLR
Proposed method	✓	✓	✓	✓	✓	GLR

Abbreviations: EWMA, exponentially weighted moving average; GLR, generalized likelihood ratio; I/MR, Individual moving range; SPE, squared prediction error.

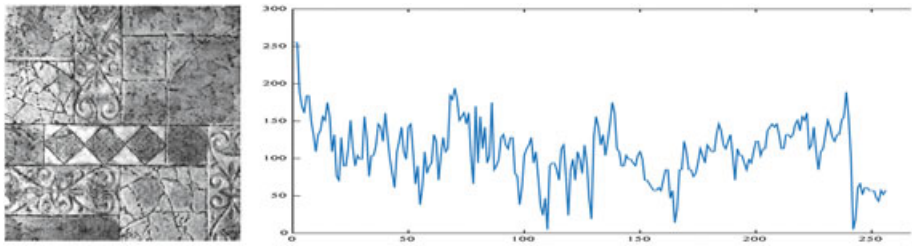

(A) (B)

FIGURE 2 A, a tile image; B, first row profile of intensity matrix [Colour figure can be viewed at wileyonlinelibrary.com]

ε_i is the error term, and $f(x_i)$ is the regression term. In nonparametric regression, this equation should be rewritten as

$$Y_i = X\beta_i + \varepsilon_i, \tag{2}$$

where β_i is vector of coefficients and X is basis function, which can be substituted by Fourier, wavelet, spline, or kernel. In our proposed method, we applied wavelet because of its proper capabilities that will be discussed later in this section. The coefficients are estimated to minimize a penalty function. Nikoo and Noorossana[20] applied a penalty function as follows:

$$PENSSE\left(\hat{f}(x),\lambda\right) = \sum_{i=1}^{n}\left(Y_i - \hat{f}(x_i)\right)^2 + \lambda\sum_{i=1}^{n}\left(\hat{f}^2(x_i)\right)^2. \tag{3}$$

$\hat{f}(x_i)$ is reconstructed function based on estimated coefficients. Parameter λ is a smoothing parameter and $\sum_{i=1}^{n}\left(\hat{f}^2(x_i)\right)^2$ is a roughness penalty term that encourages smoothness of estimation. $\sum_{i=1}^{n}\left(Y_i - \hat{f}(x_i)\right)^2$ is squared difference between the original and estimated signals (functions). This term encourages the accuracy of estimation.

As changes in each signal can follow a large class of functions, applying wavelets can be useful for parameter estimation in such an instance (Chicken et al[21]). Wavelets have property of spatial adaptivity, and as a result, they can be used for multi-resolution analysis and accurate estimation and representation of signals without any restricting assumption about their form over time. Moreover, wavelets can be applied to functions in which sharp changes, nondifferentiable points, and jumps are present where other basis functions especially spline are not proper due to over smoothing of functions or neglecting important features of the main function in the smoothing process. In some applications of wavelet transformation, analysis is conducted using a thresholding method on wavelet coefficients. Readers are referred to Chicken[19] and Chicken and Cai.[22] In these studies, the wavelet coefficients are estimated through discrete wavelet transform and after that, a thresholding rule is applied to remove noises and estimate the main denoised function. Some studies including Jin and Shi,[23] Vidakovic,[24] and Daubechies[25] applied wavelets to detect profile changes. They all applied discrete wavelet transform and compared the estimated coefficients over time.

Vidakovic[24] presented a detailed introduction on wavelet methods and their properties. Wavelet has 2 functions named as father and mother represented by ϕ and ψ, respectively. There are many options available for these 2 functions such as "haar," "Daubechies," and "Mexican hat." Each of these basis functions has its own properties and may perform different according to the case under consideration.

The main focus of this manuscript is to propose an approach based on wavelet transformation and discuss about the effect of frequency domain features in detection and diagnosis. Hence, the most prevalent and widely used basis function named as "haar" is applied in our proposed method. Moreover, computational simplicity is one of the key factors of tuning the parameters such as basis function due to large dimensions of the data. Hence, haar basis function seems suitable with respect to the computational time for high dimensional data. See Daubechies[25] for comprehensive introduction of alternative basis functions and their properties. Let $\phi_{jk}(x) = 2^{j/2}\phi(2^j x - k)$ and $\psi_{jk}(x) = 2^{j/2}\psi(2^j x - k)$ be the translation and dilation of ϕ and ψ, respectively. Each function f can be re-expressed by an infinite series as

$$f(x) = \sum_k \xi_{j0k}\phi_{j0k}(x) + \sum_{j=j_0}^{\infty}\sum_k \theta_{jk}\psi_{jk}(x), \tag{4}$$

where ξ_{jk} and θ_{jk} are inner products of f with wavelet basis functions ϕ_{jk} and ψ_{jk}, respectively. J is the level of decomposition.

One of the most useful properties of wavelets is analyzing a function in both spatial and frequency domains. This task is conducted by decomposing function to father wavelet and a number of mother wavelets. Father wavelet that is called as approximation coefficients performs as a low-pass filter and deals with low frequency and smooth part of a function. On the other hand, mother wavelet that is referred to as detail coefficients is a high-pass filter and deals with high frequency changes and detailed part of the function. Figure 3 illustrates the procedure of function segmentation with wavelets.

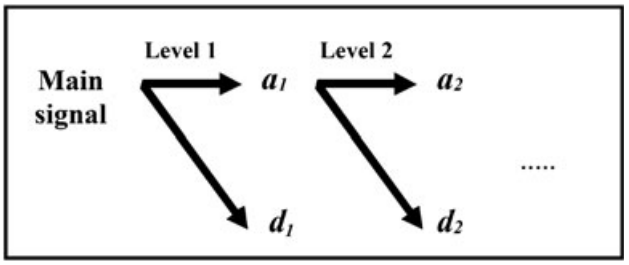

FIGURE 3 Signal decomposition by wavelets

As shown in Figure 3, for the first decomposition, each signal is decomposed into an approximation part (a_1) and a detail part (d_1). For next level of decomposition, predefined a_1 is decomposed to a new approximation part (a_2) and a detail part (d_2). This process should be continued to a level that the approximation part still has useful information about the main signal with less number of coefficients. The approximation part will be more similar to the main signal, and the number of coefficients is larger with lower decomposition levels. Hence, there exists a trade-off between the number of coefficients and similarity of approximation part to the main signal. Decomposition level selection depends on 2 factors of computational time and minimum fault region to be detected. Computational time should be equal to or less than the process cycle time to enable the monitoring procedure to be applied to 100% online inspection. Decomposition level should be smaller to make the algorithm more sensitive and to detect smaller fault sizes. On the other hand, number of coefficients and computational time will reduce by using larger decomposition levels. Hence, the level of decomposition should be smartly selected according to accuracy and computational time limitations.

As mentioned before, in many applications, the estimated coefficients are compared to a predetermined threshold and coefficients smaller than the threshold are set equal to 0. This procedure is called as wavelet denoising. In another type of applications, only approximation coefficients of last decomposition level are taken into account. This sort of application is called as data compression. Each sustained shift implemented on the image space will influence on low frequency coefficients and as a result, we consider only approximation part of the last decomposition for our further analysis in the proposed method. This could lead to dimension reduction of data and saving the computational time.

3 | THE PROPOSED METHOD

Our proposed method consists of the following steps:

3.1 | Image acquisition using MVS

It is assumed that successive online images from products of an industrial process are readily available by a MVS.

3.2 | Image preprocessing

A preprocessing step consists of transforming red, green, blue (RGB) images to gray scale, eliminating useless parts from image, resizing image to a predetermined number of pixels, contrast enhancement, and eliminating image background is needed to make images usable for our simulation study. It should be noted that these steps are considered on the basis of our capture device and the process and production line we want to monitor. Hence, performing some of these preprocessing steps may be unnecessary in new MVS devices and for other industrial cases. Moreover, in our case, images derived from the production line are all aligned and this alignment is ensured using a simple jig. In other cases, a preprocessing step called image registration may be needed to align the images and compare them to each other. There are many methods and contributions developed in the area of image de-noising, de-blurring, and registration where based on each case, researchers may apply them. Refer to Qiu[26] for more information on image processing and preprocessing techniques.

In the simulation studies, a white noise is added to each pixel's intensity that follows $\varepsilon_{ij} \sim NID(0, \sigma^2)$, which is a common assumption in SPC and profile monitoring context. Hence, a number of in-control images are generated as follows:

$$\hat{y}_{ij} = y_{ij} + \varepsilon_{ij} \quad i = 1, 2, \ldots, n \quad j = 1, 2, \ldots, n, \tag{5}$$

where y_{ij} is the intensity of original pixel located in (i,j), $\hat{y}_{ij}$is the intensity after adding noise, ε_{ij} is the white noise, ij are counters for rows and columns of image intensity matrix and n is number of rows and columns of the re-sized image after pre-processing. Hence in matrix form, it can be written as follows:

$$\hat{\mathbf{Y}} = \mathbf{Y} + \boldsymbol{\varepsilon}. \tag{6}$$

Each simulated image or real image acquired from the process is subtracted from the nominal image to make the images less redundant to correlation structure. The nominal image is considered as the image of in-control product. Hereafter, the word "image" stands for the subtracted image from the nominal image in the manuscript. Hence, only ε_{ij}'s are to be monitored over time, which are assumed to be independently and identically distributed random variables. As a result, there is no assumption about the correlation structure of the images acquired from the production line or by simulation.

3.3 | Transforming the 2D gray scale image to a number of 1D signals

There are a number of methods for transforming a 2D matrix to a number of 1D vectors such as zigzag approach, sweep line algorithm, and linear approach. The latter is implemented in our proposed method due to its simplicity and low computational time. In this approach, each row of the 2D matrix is considered as a 1D vector.

A 2D gray scale image is considered as a set of 1D signals to make 1D profile monitoring techniques applicable in the analysis of image data. For this purpose, each row of preprocessed image is considered as a nonlinear profile. Consider a $P \times Q$ gray scale image where $p = 1, 2, \ldots, P$ is row counter and $q = 1, 2, \ldots, Q$ is column counter. Figure 4 illustrates the decomposition procedure of an image into a number of 1D signals.

3.4 | Parameter estimation for each signal using 1D wavelet transformation

After estimating approximation coefficients for each profile by wavelet transformation, which is described is Section 2, a vector consists of all approximation coefficients for the whole image space is deduced as follows:

$$V = [\beta_{11}, \beta_{12}, \ldots, \beta_{1d}, \beta_{21}, \beta_{22}, \ldots, \beta_{2d}, \ldots, \beta_{P1}, \beta_{P2}, \ldots, \beta_{Pd}]. \quad (7)$$

d is number of coefficients for each signal (row), which is determined by the level of decomposition introduced before. The parameter β_{ik} is the k^{th} approximation coefficient for the ith row of image intensity matrix. So β_{11} to β_{1d} are related to the first row of image intensity matrix. The coefficients β_{21} to β_{2d} are related to the second row and so on. For each row, each approximation coefficient represents q/d of pixels. This localization property helps experimenters to determine fault location after each signal in monitoring of vector V over time by specifying the changed coefficients. All of the coefficients are equivalently important because after implementing wavelet transformation on each row, d approximation coefficients will represent that row. Hence, if a fault occurs in any region of the image, 1 or more coefficients will be changed and this change may be detected by the proposed control charting approach. It should be pointed out that it is possible to make our proposed method more sensitive in a special location of the image space. For example, one may need to detect smaller faults and make the algorithm more sensitive in the center of the image compared to the edges. For this purpose, smaller decomposition levels should be applied in the center lines and larger ones in the first and last group of lines. This leads to derive larger number of approximation coefficients for the center lines and make the algorithm more sensitive in that special region. In that case, although the coefficients are not equivalently distributed and the decomposition level varies among the rows of image intensity matrix, the proposed approach can manipulate the case without any modification because the proposed statistic, which will be discussed later in this section (step 5), compares each coefficient only to its counterpart in the nominal image.

3.5 | Monitoring the approximation coefficient over time using a GLR control chart

A multivariate control chart should be applied in this step to monitor the process over time. As mentioned before, performances of traditional multivariate control charts such as Hoteling T^2 or multivariate exponentially weighted moving average (MEWMA) are deteriorated as the number of parameters to be monitored over time increases. In image data monitoring, number of important features (approximation wavelet coefficients in this paper) that are used in SPC procedure may be from hundreds to thousands based on the sensitivity level of feature extraction algorithms. These coefficients should be monitored over time independently, ie, each coefficient derived from the main image should be monitored separately. This could help us find the parameter(s) that makes the monitoring statistic exceeds the upper control limit (UCL) and help practitioners find physical fault location in the image space after each signal that is of great importance for practitioners.

Hence, a control chart should be applied that can handle large number of coefficients over time without a significant decrease in its performance. One of these control charts is

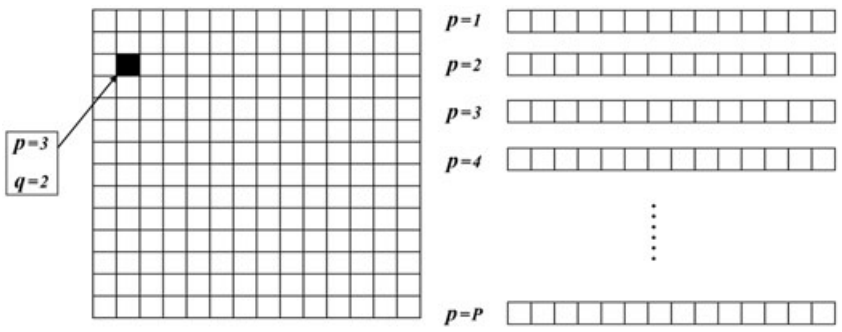

FIGURE 4 Image segmentation to 1-dimensional signals

GLR, which uses the following statistic (Reynolds and Lou[27]):

$$R_{m,s}=\begin{cases}\max\limits_{0\le\tau<S,k}\dfrac{(S-\tau)}{2\sigma_k^2}\left(\widehat{\beta}_{1,\tau,S}(k)-\beta_{0,k}\right)^2 & s=1,2,\ldots,m\\ \max\limits_{S-m\le\tau<S,k}\dfrac{(S-\tau)}{2\sigma_k^2}\left(\widehat{\beta}_{1,\tau,S}(k)-\beta_{0,k}\right)^2 & s=m+1,m+2,\ldots,\end{cases} \tag{8}$$

Because of computational time limitations, m is considered to be the window size. It means that each image is compared only to its m previous images. As a result, this control scheme can provide the change point estimation that could be an important diagnostic information for practitioners. S is image number and τ is change point. $\widehat{\beta}_{1,\tau,S}(k)$ is equal to $(s-\tau)^{-1}\sum_{t=\tau+1}^{S}\widehat{\beta}_{t,k}$ where $\widehat{\beta}_{t,k}$ is the k^{th} element of V vector for the t^{th} sample. $\beta_{0,k}$ is the kth element of V vector for nominal image, and σ_k^2 is the variance of k^{th} coefficient computed by phase I data. To summarize the above discussion, out-of-control signal, fault location in image space, and change point estimation are achieved simultaneously by applying GLR control chart. These results help practitioners find root causes of the change and provide valuable diagnostic information to recover the process to its in-control status.

3.6 | Performance evaluation of the proposed method

Performance evaluation is done using 3 groups of metrics. First group deals with computing the number of observations between a shift implementation and a signal from the proposed procedure. Average run length (ARL) and standard deviation of run lengths are computed to show the effectiveness of the proposed method in detecting faults as quickly as possible. Second group of metrics study the preciseness of change point estimation by the proposed method. Difference between estimated change point ($\widehat{\tau}$) and real change point (τ) is used to compute the accuracy of change point estimation ($\varepsilon=\widehat{\tau}-\tau$). Last metric evaluates the preciseness of the proposed method in detecting fault location. Sorensen dice similarity coefficient (SDSC) is applied to compare the estimated and real fault locations. This coefficient is computed as

$$SDSC=\frac{2\times(A\cap B)}{A+B}, \tag{9}$$

where A is the specified fault location by the proposed method and B is the real fault location. This metric will be 1 if A and B are quite the same and 0 if A and B have no overlap. In other circumstances, SDSC will be between 0 and 1. Figure 5 shows a flowchart that illustrates the procedure for our proposed approach.

4 | SIMULATION STUDY

Our simulation studies will be described according to subsections explained in the previous section. For the first step, a 3264×2448 pixel image from a tile is derived from the MVS as shown in Figure 6.

Second step deals with preprocessing. In this step, RGB image will be transformed to gray scale image. Moreover, images are resized to 256×256pixels. One of the preprocessing steps is rescaling the intensity matrix (I) of the image. In the original image, intensity of each pixel is a number between 0 (black) and 255 (white). This preprocessing step rescales the data and transforms the pixels' intensities to numbers between 0 and 1 by dividing each number by 255. Result is an intensity matrix (I') in which each element is a number between 0 and 1 ($I'=I./255$). A contrast enhancement is performed on the image, and the resulted image can be considered as the nominal image shown in Figure 7.Afterwards, 1000 in-control images are generated by adding white noise to the nominal image. If a number of in-control real images are available from the production line, one of them can be considered as nominal image and other in-control images should be applied as phase I data. This procedure is applied for the case study and will be discussed in Section 5.

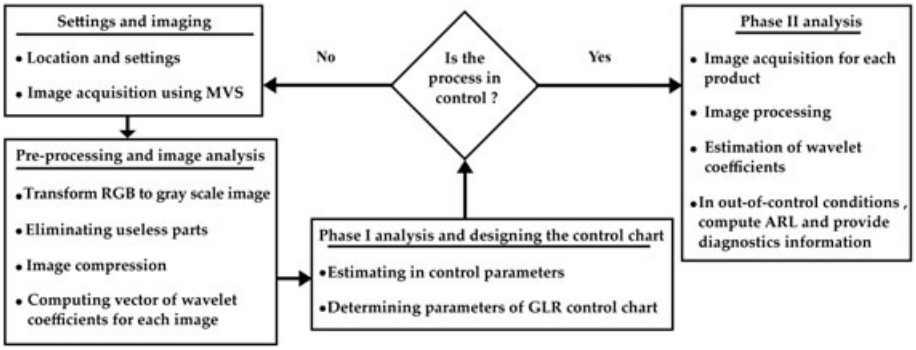

FIGURE 5 Flowchart for the procedure of the proposed scheme. GLR, generalized likelihood ratio; MVS, machine vision system.

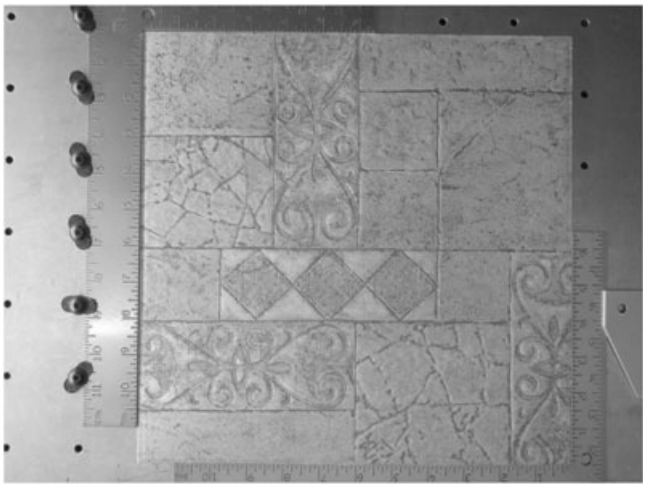

FIGURE 6 Original tile image derived from the machine vision system

FIGURE 7 The nominal image after preprocessing

Many noise types such as Poisson, salt and pepper, or Gaussian noise can be added as white noise to the nominal image to generate in-control phase I data. A zero-mean Gaussian distribution with standard deviation equal to .01 is considered in our simulation studies. As mentioned before, in one of the preprocessing steps, the intensity matrix is rescaled. Hence, .01 is the standard deviation which is implemented on $I^{'}$. It means that the original standard deviation is $\sigma_0 = 255 \times 0.01 = 2.55$. Considering larger amounts for white noise standard deviation leads to contamination of defected and nondefected images and losing the chance to detect out-of-control conditions. For determining the correct amount for white noise standard deviation, signal-to-noise ratio (SNR) should be computed as Equation 10:

$$SNR = 10\log_{10}\frac{\mathrm{var}(f(x))}{\sigma_0^2}, \tag{10}$$

where var($f(x)$) is the variance of intensity matrix and σ_0^2 is the variance of white noise. Nonparametric methods perform well for $SNR \geq 25$ (Chicken[19]). In our case, var($f(x)$) $= 0.0437$ and $\sigma_0^2 = 0.0001$. Under these considerations, *SNR* is equal to 26.407. It is obvious that larger amounts of *SNR* lead to better performance of the proposed approach.

Since our preprocessed image size is 256×256, each main signal—each line of image intensity matrix—has 256 elements. For example, when decomposition level is equal to 4, the last approximation part consists of 16 coefficients. Hence, each coefficient represents 16 elements of the main signal. The decomposition process is shown in Figure 8.

Figure 9 shows the nondefective image (left) and defective image (right) with their first row profile at the bottom of each image.

As shown in Figure 9, the coefficient (dotted circle) that is related to the defected area is different from its counterpart in the in-control vector of coefficients. It should be noted that shift is implemented on 17th to 32nd pixels, which are related to second coefficient. As mentioned before, in the fourth decomposition level of wavelet transformation, 16 approximation coefficients are derived from each main 1D signal, which includes 256 pixel intensities. Each coefficient represents 16 intensities of the original signal. Thus, first coefficient represents first to 16th elements, second coefficient represents 17th to 32nd elements, and so on. Hence, when only 17th to 32nd pixels of a row in image intensity matrix are defected, only second coefficient will change and other coefficients remain unchanged. This localization property of wavelet transformation helps practitioners find the physical fault location in the image space after each out-of-control signal.

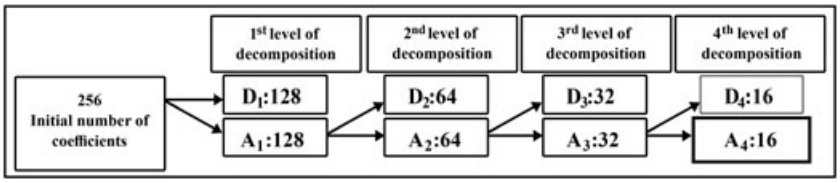

FIGURE 8 Decomposition procedure of each signal

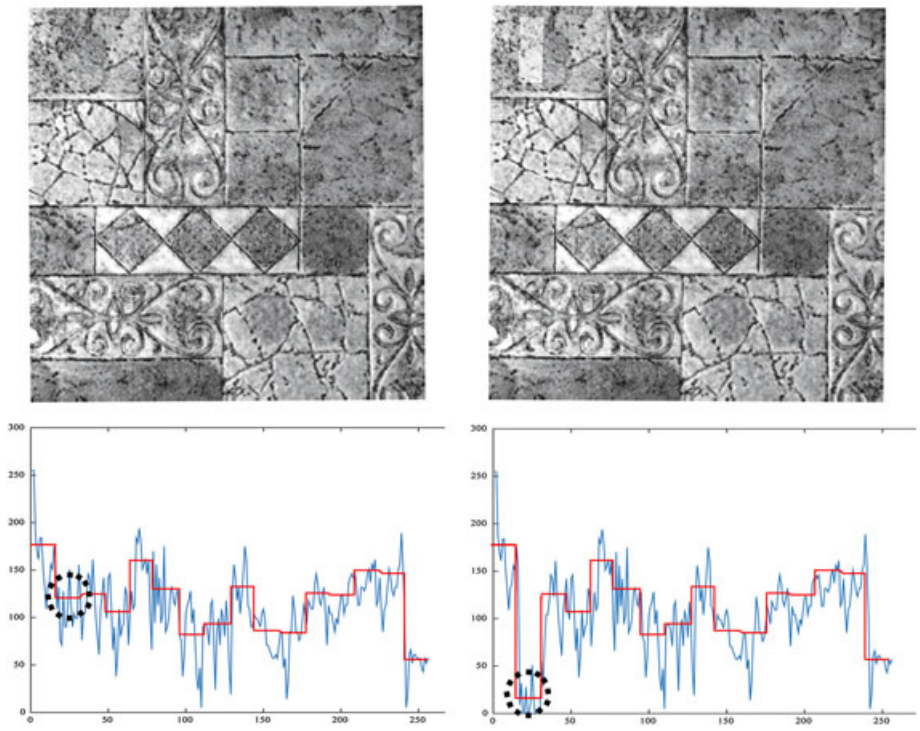

FIGURE 9 Changes in the second coefficient of first row after shift [Colour figure can be viewed at wileyonlinelibrary.com]

After generating phase I images, the UCL of the GLR control chart is computed as 13.69 by simulation studies with 10 000 runs while considering in-control ARL of 200.

In phase II, images with various sustained shifts in the intensities of pixels are generated. In our simulation study, a step change is occurred after change point(τ). We set τ equal to 5 that means that in each replication, a step change is occurred from the sixth image. This helps us achieve steady state ARL for evaluation of the proposed method fault detection capability. The proposed method is tested under 120 fault testing conditions (2 shift centers $\times$20 shift magnitudes (Δ) $\times$3 fault sizes).

Minimum fault region is considered as a 5×5 region in our simulation studies. So, in each defected signal, the intensities of at least 5 pixels are changed. Two scenarios are considered as the best and worst cases. The worst case is when 3 of these changed intensities appear in 1 region and the other 2 intensities in the adjacent region. On the other hand, best case is occurred when all of the defected pixels influence 1 coefficient. Figure 10 clarifies the best and worst scenarios that can occur in a 5×5 fault size.

As illustrated in Figure 10, at least 2/16 of the main signal intensities for each coefficient will change in a 5×5 fault region. It is obvious that for smaller decomposition levels, the number of coefficients for each main signal will increase. For example, when decomposition level is set to 3, 32 coefficients will represent the main signal and as a result, each 8 pixels have a unique representative. Hence, changing of 2 intensity pixels (2/8 of data for the related coefficient) will influence more on the coefficient and as a result, coefficients are more sensitive to intensity fluctuations. This will lead to faster signals and improvement in the evaluation metrics but computational time will increase. On the other hand, for decomposition level equal to 5, each 32 pixels are summarized into 1 coefficient. Hence, change of 2 pixels' intensities, 2/32 of the data related to the coefficient are changed. This will reduce the computational time but practically, faults are hard to detect and might be neglected under this setting. If the smallest fault size to be detected is considered as a larger area, it may be appropriate to set the decomposition level equal to 5. In our simulation study, the decomposition level is set equal to 4 based on trial and error while analyzing the

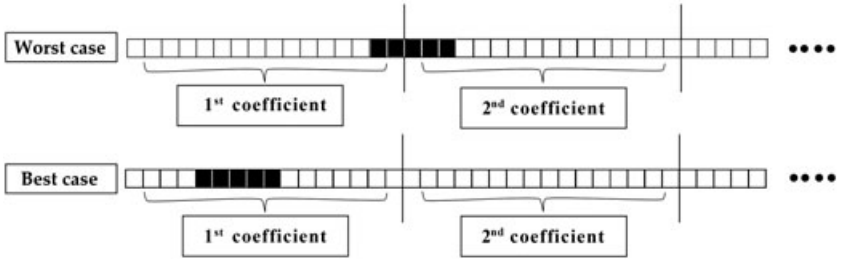

FIGURE 10 Best and worst scenarios for the simulation studies

TABLE 2 Simulation results for 5×5 fault size

		Detection Power		Change Point Estimation ($\varepsilon = \hat{\tau} - \tau$)						Physical Fault Location			
Fault Center	Δ	*ARL*	*std* (*RL*)	*med*(ε)	*E* (ε)	*std* (ε)	ε = 0 (%)	0 < |ε| ≤ 2	|ε| > 2	*E* (*SDSC*)	*std* (*SDSC*)	*E* (*JSDS*)	*std* (*JSDS*)
[5, 5] (best case)	+10	1.05	0.24	0.00	−0.01	0.16	98.85	1.10	0.05	0.22	0.03	0.91	0.12
	+9	1.21	0.41	0.00	−0.02	0.15	98.40	1.60	0	0.21	0.03	0.86	0.15
	+8	1.48	0.51	0.00	−0.02	0.16	97.70	2.30	0	0.20	0.04	0.84	0.18
	+7	1.78	0.50	0.00	−0.04	0.31	95.10	4.70	0.20	0.20	0.05	0.82	0.20
	+6	2.31	0.63	0.00	−0.09	0.51	89.45	9.55	1.00	0.19	0.05	0.79	0.20
	+5	3.05	0.87	0.00	−0.07	0.67	83.10	15.20	1.70	0.17	0.05	0.73	0.21
	+4	4.42	1.32	0.00	−0.09	0.99	69.25	26.60	4.15	0.16	0.05	0.68	0.22
	+3	7.33	2.60	0.00	0.44	1.78	52.60	36.90	10.50	0.15	0.05	0.62	0.23
	+2	27.83	22.71	13.00	20.29	22.80	7.90	10.00	82.10	0.14	0.07	0.58	0.29
	+1	161.38	163.43	10.00	157.03	163.19	0.50	1.80	97.70	0.01	0.02	0.05	0.09
	−1	169.13	176.13	109.00	164.79	176.07	0.60	2.00	97.40	0.01	0.09	0.03	0.08
	−2	24.21	19.38	14.00	21.82	24.47	9.50	16.00	74.50	0.09	0.05	0.40	0.21
	−3	6.81	2.45	0.00	0.28	1.53	52.40	37.30	10.30	0.15	0.06	0.61	0.23
	−4	4.47	1.29	0.00	−0.07	0.93	69.60	27.10	3.30	0.16	0.05	0.68	0.22
	−5	3.09	0.83	0.000	−0.11	0.72	80.60	17.70	17.00	0.17	0.05	0.72	0.21
	−6	2.28	0.64	0.00	−0.09	0.57	89.10	9.60	1.30	0.18	0.05	0.77	0.21
	−7	1.83	0.53	0.00	−0.03	0.29	95.10	4.70	0.20	0.20	0.05	0.82	0.19
	−8	1.55	0.51	0.00	−0.03	0.28	96.95	2.80	0.25	0.20	0.04	0.85	0.18
	−9	1.25	0.44	0.00	−0.02	0.16	98.45	1.50	0.05	0.21	0.04	0.87	0.15
	−10	1.05	0.23	0.00	−0.02	0.17	98.80	0.10	1.10	0.22	0.03	0.91	0.13
[128, 128] (worst case)	+10	2.39	0.66	0.00	−0.09	0.60	88.30	10.00	1.70	0.09	0.02	0.63	0.17
	+9	2.80	0.78	0.00	−0.10	0.67	83.40	15.20	1.40	0.08	0.02	0.61	0.17
	+8	3.35	0.95	0.00	−0.15	0.81	77.10	21.00	1.90	0.08	0.02	0.58	0.17
	+7	4.19	1.22	0.00	−0.10	0.95	68.10	27.90	4.00	0.07	0.02	0.55	0.18
	+6	5.47	1.64	0.00	−0.04	1.18	63.30	30.40	6.30	0.07	0.03	0.53	0.18
	+5	7.45	2.77	0.00	0.55	2.19	47.10	38.40	14.50	0.07	0.02	0.48	0.18
	+4	13.46	8.54	2.00	5.64	8.23	20.50	28.10	51.40	0.05	0.02	0.39	0.16
	+3	50.59	44.94	29.00	43.02	44.86	2.40	4.70	92.90	0.03	0.02	0.23	0.14
	+2	141.29	134.71	98.00	136.12	134.67	1.00	2.70	96.30	0.01	0.01	0.05	0.08
	+1	186.67	179.67	124.00	182.34	179.56	0.30	1.70	98.00	0.00	0.01	0.01	0.03
	−1	184.49	179.35	125.00	179.85	179.47	0.50	1.50	98.00	0.00	0.01	0.01	0.03
	−2	139.45	140.96	86.00	134.03	140.90	0.60	2.60	96.80	0.09	0.01	0.06	0.09
	−3	42.57	37.59	24.00	35.13	37.46	3.80	6.00	90.20	0.03	0.02	0.24	0.14
	−4	13.15	7.78	2.00	5.17	7.49	21.40	28.60	50.00	0.05	0.02	0.41	0.16
	−5	7.47	2.87	0.00	0.53	2.16	48.90	35.70	15.40	0.07	0.02	0.50	0.19
	−6	5.45	1.65	0.00	0.02	1.11	62.50	32.10	5.40	0.07	0.02	0.54	0.18
	−7	4.19	1.19	0.00	−0.07	0.95	72.50	23.30	4.20	0.08	0.02	0.57	0.18
	−8	3.39	0.99	0.00	−0.09	0.78	79.90	18.00	2.10	0.08	0.02	0.59	0.18
	−9	2.75	0.77	0.00	−0.09	0.58	85.60	13.40	1.00	0.08	0.02	0.62	0.17
	−10	2.41	0.66	0.00	−0.08	0.58	86.30	12.90	0.80	0.09	0.02	0.65	0.17

Abbreviations: ARL, average run length; JSDS, justified Sorensen dice similarity coefficient; SDSC, Sorensen dice similarity coefficient; std, standard deviation.

computational time and evaluating the metrics. It is recognized that this decomposition level leads to suitable performance of the proposed method in detecting 5×5 or larger fault sizes.

All of the fault regions considered in our study are squared shaped of sizes 5×5, 10×10, and 15×15. Worst and best cases can be extended for 10×10 and 15×15 fault regions. Hence, there will be no difference if columns are considered as 1D signals instead of rows. This is because of the nature of GLR control chart that monitors each coefficient independent from the others. Therefore, for a 1×5 fault region, there are 1 (best case) or 2 (worst case) affected coefficients and these coefficients can be determined by the proposed wavelet based method as exactly as a 5×5 fault size.

In a squared shaped fault, the same number of rows and columns would be affected and as a result, the performance of the proposed method will not be different in each case.

TABLE 3 Simulation results for 10×10 fault size

		Detection Power		Change Point Estimation ($\varepsilon = \widehat{\tau} - \tau$)						Physical Fault Location			
Fault Center	**Δ**	***ARL***	***std*(*RL*)**	***med*(ε)**	***E*(ε)**	***std*(ε)**	**ε = 0 (%)**	**0 < |ε| ≤ 2**	**|ε| > 2**	***E* (*SDSC*)**	***std* (*SDSC*)**	***E* (*JSDS*)**	***std* (*JSDS*)**
[5, 5]	+10	1.00	0.00	0.00	0.00	0.00	100.00	0.00	0.00	0.38	0.00	1.00	0.00
(best case)	+9	1.00	0.00	0.00	0.00	0.00	100.00	0.00	0.00	0.38	0.00	1.00	0.00
	+8	1.00	0.00	0.00	0.00	0.00	100.00	0.00	0.00	0.38	0.00	1.00	0.00
	+7	1.00	0.00	0.00	0.00	0.03	99.90	0.10	0.00	0.38	0.01	1.00	0.01
	+6	1.00	0.00	0.00	0.00	0.03	99.90	0.10	0.00	0.38	0.01	0.99	0.03
	+5	1.00	0.00	0.00	−0.0`	0.09	99.40	0.60	0.00	0.35	0.03	0.92	0.08
	+4	1.24	0.43	0.00	−0.02	0.21	98.10	1.70	0.20	0.31	0.05	0.80	0.14
	+3	1.93	0.48	0.00	−0.07	0.48	90.80	8.30	0.90	0.29	0.07	0.75	0.19
	+2	3.61	1.01	0.00	−0.13	0.85	75.20	22.40	2.40	0.24	0.08	0.64	0.20
	+1	16.73	10.65	5.00	8.74	10.47	13.70	19.20	67.10	0.16	0.07	0.41	0.18
	−1	17.32	12.37	5.00	9.48	12.06	14.30	20.60	65.10	0.15	0.07	0.38	0.17
	−2	3.72	1.08	0.00	−0.08	0.81	77.00	20.70	2.30	0.25	0.07	0.65	0.20
	−3	1.93	0.53	0.00	−0.09	0.47	92.10	6.80	1.10	0.28	0.07	0.73	0.19
	−4	1.25	0.44	0.00	−0.03	0.20	96.70	3.20	0.10	0.31	0.06	0.80	0.15
	−5	1.01	0.08	0.00	−0.01	0.17	99.50	0.40	0.00	0.35	0.03	0.92	0.08
	−6	1.00	0.00	0.00	0.00	0.00	100.00	0.00	0.00	0.378	0.01	0.98	0.04
	−7	1.00	0.00	0.00	0.00	0.00	100.00	0.00	0.00	0.38	0.00	1.00	0.01
	−8	1.00	0.00	0.00	0.00	0.00	100.00	0.00	0.00	0.38	0.00	1.00	0.00
	−9	1.00	0.00	0.00	0.00	0.00	100.00	0.00	0.00	0.38	0.00	1.00	0.00
	−10	1.00	0.00	0.00	0.00	0.00	100.00	0.00	0.00	0.38	0.00	1.00	0.00
[128, 128]	+10	1.00	0.00	0.00	−0.01	0.12	98.90	1.10	0.00	0.22	0.01	0.91	0.06
(worst case)	+9	1.01	0.01	0.00	−0.02	0.17	98.20	1.70	0.10	0.20	0.02	0.84	0.08
	+8	1.12	0.32	0.00	−0.02	0.13	96.90	2.50	0.60	0.18	0.03	0.77	0.11
	+7	1.47	0.50	0.00	−0.08	0.45	94.30	4.70	1.00	0.18	0.04	0.75	0.17
	+6	1.81	0.48	0.00	−0.08	0.47	92.40	6.70	0.90	0.17	0.04	0.71	0.17
	+5	2.33	0.63	0.00	−0.11	0.67	84.10	14.30	1.60	0.15	0.04	0.65	0.18
	+4	3.30	0.90	0.00	−0.15	0.89	74.80	22.20	3.00	0.14	0.04	0.59	0.18
	+3	5.21	1.49	0.00	−0.07	1.27	56.60	36.30	7.10	0.12	0.04	0.52	0.18
	+2	12.53	6.79	2.00	4.64	6.43	21.50	28.10	50.40	0.09	0.04	0.39	0.15
	+1	133.79	133.87	88.00	128.23	130.91	1.00	2.70	96.30	0.01	0.01	0.06	0.06
	−1	115.56	114.46	74.50	109.89	114.40	0.70	2.40	96.90	0.02	0.01	0.07	0.06
	−2	12.21	6.72	2.00	4.47	6.41	21.10	28.90	50.00	0.09	0.04	0.39	0.16
	−3	5.09	1.46	0.00	−0.11	1.26	56.60	36.00	7.40	0.12	0.04	0.52	0.18
	−4	3.21	0.89	0.00	−0.13	0.83	75.30	21.90	2.80	0.14	0.04	0.59	0.18
	−5	2.30	0.63	0.00	−0.12	0.64	86.20	12.10	1.70	0.16	0.04	0.66	0.18
	−6	1.79	0.47	0.00	−0.08	0.45	92.40	7.00	0.60	0.17	0.04	0.72	0.18
	−7	1.48	0.50	0.00	−0.05	0.33	94.90	4.70	0.40	0.18	0.04	0.75	0.17
	−8	1.11	0.31	0.00	−0.03	0.27	97.10	2.70	0.20	0.18	0.03	0.77	0.11
	−9	1.01	0.71	0.00	0.02	0.14	98.20	1.80	0.00	0.20	0.02	0.84	0.08
	−10	1.00	0.00	0.00	−0.01	0.14	99.00	0.90	0.10	0.22	0.01	0.91	0.06

Abbreviations: ARL, average run length; JSDS, justified Sorensen dice similarity coefficient; SDSC, Sorensen dice similarity coefficient; std, standard deviation.

For a 2×10 fault region, only 2 rows are affected but 10 columns will change. In this scenario, there are 10 affected intensities in each of the 2 rows but if we consider columns, 2 elements of each column are changed that may be neglected by the statistic. As a matter of fact, row decomposition also seems to perform better in this scenario.

In vertical faults, the performance of the proposed method will be deteriorated for fault widths smaller than 3. For example in a 5×1 fault, only 1 pixel from the forming pixels of a coefficient (1/16 of the data) is affected and this change cannot be detected by the proposed method unless using a smaller decomposition level. Row decomposition can be substituted by column decomposition to improve the performance of the proposed scheme for detecting vertical fault areas. In other words, considering each column as a 1D signal instead of each row makes the proposed scheme more sensitive to vertical changes with narrow widths. In general, any decomposition method can be substituted by

TABLE 4 Simulation results for 15×15 fault size

Fault Center	Δ	Detection Power		Change Point Estimation ($\varepsilon = \hat{\tau} - \tau$)						Physical Fault Location			
		ARL	*std*(*RL*)	*med*(ε	*E*(ε)	*std*(ε)	ε = 0 (%)	0 < |ε| ≤ 2	|ε| > 2	*E*(*SDSC*)	*std*(*SDSC*)	*E*(*JSDS*)	*std*(*JSDS*)
[7, 7]	+10	1.00	0.00	0.00	0.00	0.00	100.00	0.00	0.00	0.97	0.00	1.00	0.00
(best case)	+9	1.00	0.00	0.00	0.00	0.00	100.00	0.00	0.00	0.97	0.00	1.00	0.00
	+8	1.00	0.00	0.00	0.00	0.00	100.00	0.00	0.00	0.97	0.00	1.00	0.00
	+7	1.00	0.00	0.00	0.00	0.00	100.00	0.00	0.00	0.97	0.00	1.00	0.00
	+6	1.00	0.00	0.00	0.00	0.00	100.00	0.00	0.00	0.97	0.00	1.00	0.00
	+5	1.00	0.00	0.00	0.00	0.00	100.00	0.00	0.00	0.97	0.01	0.99	0.01
	+4	1.00	0.00	0.00	0.00	0.03	99.90	0.10	0.00	0.95	0.03	0.99	0.03
	+3	1.01	0.08	0.00	−0.01	0.16	98.80	0.11	0.10	0.84	0.08	0.87	0.08
	+2	1.82	0.48	0.00	−0.08	0.44	93.60	5.70	0.70	0.72	0.17	0.74	0.18
	+1	5.28	1.55	0.00	−0.11	1.29	57.40	3.58	6.80	0.53	0.18	0.54	0.19
	−1	5.40	1.62	0.00	−0.04	1.42	55.60	3.46	9.80	0.52	0.19	0.54	0.19
	−2	1.83	0.49	0.00	−0.06	0.38	93.00	6.70	0.30	0.71	0.18	0.74	0.17
	−3	1.01	0.09	0.00	−0.01	0.08	99.40	0.60	0.00	0.84	0.07	0.87	0.07
	−4	1.00	0.00	0.00	0.00	0.06	99.70	0.30	0.00	0.95	0.03	0.99	0.03
	−5	1.00	0.00	0.00	0.00	0.00	100.00	0.00	0.00	0.97	0.01	1.00	0.00
	−6	1.00	0.00	0.00	0.00	0.00	100.00	0.00	0.00	0.97	0.00	1.00	0.00
	−7	1.00	0.00	0.00	0.00	0.00	100.00	0.00	0.00	0.97	0.00	1.00	0.00
	−8	1.00	0.00	0.00	0.00	0.00	100.00	0.00	0.00	0.97	0.00	1.00	0.00
	−9	1.00	0.00	0.00	0.00	0.00	100.00	0.00	0.00	0.97	0.00	1.00	0.00
	−10	1.00	0.00	0.00	0.00	0.00	100.00	0.00	0.00	0.97	0.00	1.00	0.00
[128, 128]	+10	1.00	0.00	0.00	0.00	0.00	100.00	0.00	0.00	0.64	0.00	1.00	0.00
(worst case)	+9	1.00	0.00	0.00	0.00	0.00	100.00	0.00	0.00	0.63	0.01	0.99	0.01
	+8	1.00	0.00	0.00	0.00	0.00	100.00	0.30	0.00	0.63	0.01	0.98	0.02
	+7	1.00	0.00	0.00	−0.01	0.08	99.70	0.30	0.00	0.60	0.02	0.94	0.04
	+6	1.00	0.00	0.00	−0.01	0.13	99.00	0.90	0.10	0.55	0.04	0.86	0.06
	+5	1.11	0.32	0.00	−0.03	0.27	98.20	1.60	0.20	0.47	0.07	0.74	0.11
	+4	1.66	0.48	0.00	−0.06	0.39	92.80	6.60	0.60	0.45	0.11	0.70	0.17
	+3	2.48	0.64	0.00	−0.16	0.70	81.50	16.40	2.10	0.39	0.10	0.61	0.16
	+2	4.59	1.33	0	−0.14	1.76	59.30	35.00	5.70	0.32	0.11	0.50	0.16
	+1	28.86	23.15	14.5	21.24	23.02	6.60	10.10	83.30	0.16	0.07	0.24	0.11
	−1	27.96	23.30	13	20.31	23.28	5.90	12.20	81.90	0.16	0.07	0.25	0.12
	−2	4.61	1.28	0.00	−0.23	1.27	59.40	32.60	8.00	0.33	0.11	0.51	0.17
	−3	2.47	0.66	0.00	−0.20	0.79	82.10	14.90	3.00	0.40	0.10	0.62	0.16
	−4	1.63	0.49	0.00	−0.06	0.35	93.60	6.20	0.20	0.45	0.11	0.71	0.17
	−5	1.12	0.33	0.00	−0.05	0.33	96.40	3.10	0.50	0.48	0.08	0.74	0.12
	−6	1.00	0.04	0.00	−0.02	0.12	98.50	1.50	0.00	0.55	0.04	0.86	0.06
	−7	1.00	0.00	0.00	0.00	0.04	99.80	0.20	0.00	0.60	0.02	0.94	0.03
	−8	1.00	0.00	0.00	0.00	0.05	99.70	0.30	0.00	0.62	0.01	0.98	0.02
	−9	1.00	0.00	0.00	0.00	0.00	100.00	0.00	0.00	0.63	0.01	0.99	0.01
	−10	1.00	0.00	0.00	0.00	0.00	100.00	0.00	0.00	0.64	0.00	1.00	0.00

Abbreviations: ARL, average run length; JSDS, justified Sorensen dice similarity coefficient; SDSC, Sorensen dice similarity coefficient; std, standard deviation.

row decomposition according to the case and user's preferences.

Results of our simulation studies are summarized in Tables 2, 3, and 4, which are related to 5×5, 10×10, and 15×15 fault sizes, respectively. The first 2 columns of each table represent ARL and standard deviation of run lengths, which are evaluation metrics for fault detection capability of the proposed method. For each fault size, 2 fault centers are considered based on best case and worst case scenarios, which have been explained before. As mentioned in Section 3, the difference between the estimated and real change points ($\varepsilon = \hat{\tau} - \tau$) is considered as the metric for evaluating the preciseness of change point estimation by the proposed method. Columns 3 to 5 of each table represent median, mean, and standard deviation of ε's. Next 3 columns compute the percent of ε's equal to 0, between zero and 2 and larger than 2. Last part of our simulation study is computing SDSC to evaluate preciseness of the proposed method in detecting fault location. As mentioned before, each 16 pixels are represented by 1 coefficient in wavelet transformation of our

simulation study. As a result, by a change in each pixel, a location consist of 16 pixels will have fluctuations. Hence, for example for a 5×5 fault region in our best case scenario, 5 coefficients are determined by the proposed method as the fault location. So, real shift area (A) is 5×5 and estimated shift area (B) is 5×16. In this case, if the procedure recognizes the 5 coefficients correct, SDSC will be equal to 0.4761, which can be computed as follows:

$$\frac{2\times(A\cap B)}{A+B}=\frac{2\times(5\times5)}{(5\times5)+(5\times16)}=0.4761.$$

This in maximum achievable SDSC under this fault testing condition and we named it as maximum achievable SDSC (MSDS).

SDSC/MSDS can be a better representation for evaluation of the proposed method in estimating the fault location. So, justified SDSC (JSDS) is computed as SDSC/MSDS. Mean and variance of SDSC and JSDS are reported in the last 4 columns of Tables 2, 3, and 4.

It can be observed that as expected, performance is better under the best case in comparison with the worst case. It can be seen that ARLs start to deteriorate for shift magnitudes (Δ) smaller than 2 ($|\Delta|\leq2$) especially for fault size of 5×5. This is expected because in worst case scenario, 2 changing pixels are related to 1 coefficient and 3 changing pixels are related to adjacent coefficient. Each coefficient represents 16 pixels. Hence, in this scenario, only 3/16 of the components of a coefficient are changed. On the other hand, shift magnitudes smaller than 2 are too small because intensity shifts smaller than 10 ($|\Delta|\leq10$) are barely visible with human eyes.

It can be seen from the tables that the change point estimator performance starts to deteriorate for intensity shifts smaller than or equal to 3 for 5×5, 2 for 10×10, and 1 for 15×15 fault sizes in the worst case scenario. In other intensity shifts, median of ε's is equal to 0 and the expected value is very small. Furthermore, the percent of ε's that are equal to 0 is more than 60% for intensity shifts larger than 5, and this value can go up to 100% for larger fault sizes and intensity shifts.

SDSC and JSDS are deteriorated for fault sizes smaller than or equal to 10×10 and intensity shifts smaller than or equal to 4 due to setting the decomposition level equal to 4.

All of these metrics can be improved if one uses a smaller decomposition level. In this case, the algorithm will be more sensitive but with each 1 decrement in decomposition level, number of deduced coefficients will be twice, and monitoring this large number of coefficients may be impossible from time and cost point of views.

We considered a competitive method proposed by Megahed et al[18] to compare our results and confirm suitable performance of the proposed method because their method also deals with gray scale images. The nominal image from textile industry that is applied in that manuscript is shown in Figure 11.

Our proposed method is applied on this data. The preprocessing steps are the same to those applied by the competitive paper. Poisson noise should be applied and only then the results can be comparable. For the image shown in Figure 11, var($f(x)$) is 0.0171 and σ_0^2 is equal to 4.3366×10^{-13} by applying Poisson noise distribution. So *SNR* is computed equal to 105.9585, which is too large in comparison to the one applied in our study. The competitive approach uses median run length (MRL) to evaluate performance. They considered in-control MRL equal to 148. Our proposed scheme is applied under these settings, and UCL is found equal to 13.73 to achieve in-control MRL the same as the competitive approach. As expected, the proposed method dominates the results reported by the competitive approach. This is due to the considered *SNR* that is equal to 26.407 in our simulation studies and larger *SNRs* lead to better performance of the proposed method. Here, even for shift magnitude equal to 1 ($\Delta=\pm1$) and a worst case 5×5 fault region, ARL is equal to 1, mean and median of $\varepsilon=\widehat{\tau}-\tau$ are 0, and JSDS is also equal to 1. Results are obtained by 10 000 runs using MATLAB 2016a.

5 | CASE STUDY

In this section, the proposed method is applied to a real case study, which is also used by Megahed et al.[18] For this purpose, 100 successive images gathered from a tile production line are analyzed. The cameras are fixed and the environment is preserved of any environmental changes. Readers are referred to Megahed et al[18] to find more details about settings and data gathering conditions. All of the settings and number

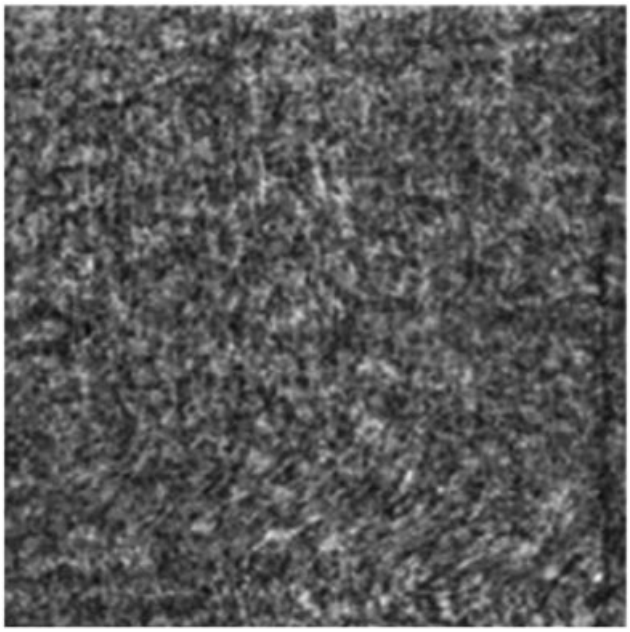

FIGURE 11 Textile nominal image

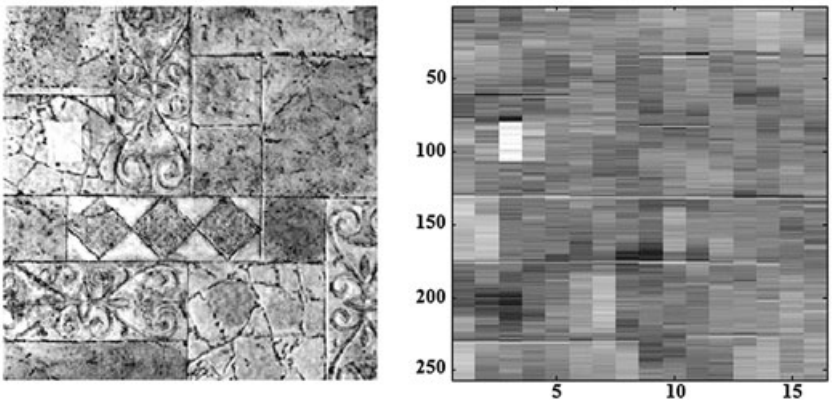

FIGURE 12 The defected tile image and affected coefficients

of images acquired for phase I are set equal to those considered by Megahed et al[18] to make the results comparable. First 41 images are considered as in-control images, and one of them is randomly selected as the nominal image. Other 40 images are considered as phase I data. As mentioned in Section 3, each image should be subtracted from the nominal image to make the images less redundant to correlation structure. It is important to say that there is no need to have a large number of real images, and only a limited number (40 images in our case) is enough, and it is possible to generate a number of in-control images based on these 40 images to estimate phase I parameters more precisely. 1000 replications are conducted to estimate phase I parameters. Images 42nd to 100th are considered as phase II evaluation data. It is assumed that the process is in-control for the next 20 images. After that, a sustained shift with magnitude of $+10$ ($\Delta = +10$) is implemented on a 30×30 region. This shift magnitude and fault size are set the same as the ones considered by Megahed et al.[18] Our proposed approach detected this shift on the 62nd image (first image after implementing the shift), but the competitive approach detected this shift on 64th image. Both methods could estimate the change point precisely on the 61st image.

A real defected image is shown in Figure 12. The shift location estimated by our proposed algorithm is illustrated in the right side of this figure. Results illustrate satisfying performance of the method in manipulating industrial cases to detect out-of-control situations along with providing precise diagnostic information about fault size/location and change point estimation.

6 | CONCLUSIONS

Image data have attracted significant and increasing attention in many real life problems in recent years. This paper proposes a contribution about applying image data in SPC context using a nonparametric profile monitoring approach. Wavelet transformation is applied for feature extraction due to its suitable properties especially localization property, which enables the proposed method to detect fault location. After feature extraction with wavelet transformation, the approximation coefficients are monitored over time using a GLR control chart. Average run length, SDSC, and $(\widehat{\tau}-\tau)$ are considered in simulation studies to evaluate the performance of the proposed method in detecting faults, determining fault location, and estimating change point, respectively. Results under different fault testing conditions indicate that the proposed method is capable of not only detecting shifts quickly but also estimating the change point and location of faults with proper level of accuracy. A comparison is conducted with the method proposed by Megahed et al,[18] and results illustrate that our proposed method can outperform their method either in small or large fault sizes and magnitudes. Moreover, the proposed method is applied on a real case from tile industry. Evaluation of the proposed method using other basis functions such as Daubechies or Mexican hat can be considered as a future research suggestion. Moreover, because of the complicated-structured data of each image, RL's have large fluctuations and UCL is found by trial and error to achieve a predetermined in-control ARL in the simulation studies. Finding in-control RL distribution for determining optimal value for UCL in various circumstances based on the probability distribution can also be considered as another appealing area of future research.

ACKNOWLEDGEMENTS

We would like to thank the anonymous reviewers for their insightful comments, which led to the improvement of the paper.

REFERENCES

1. Noorossana R, Saghaei A, Amiri A. *Statistical Analysis of Profile Monitoring*. Hoboken, NJ: John Wiley & Sons, Inc.; 2011.
2. Siew LH, Hodgson RM, Wood EJ. Texture measures for carpet wear assessment. *IEEE Trans Pattern Anal Mach Intell*. 1988;10:92-105.
3. Latif-Amet A, Ertüzün A, Erçil A. An efficient method for texture defect detection: sub-band domain co-occurrence matrices. *Image Vis Comput*. 2000;18:543-553.

4. Tico M, Kuosmanen P, Saarinen J. Wavelet domain features for fingerprint recognition. *Electron Lett*. 2001;37:21-22.
5. Sari-Sarraf H, Goddard JS Jr. Robust defect segmentation in woven fabrics. *Proc IEEE Conf Comput Vis Pattern Recognit*. 1998;938-944.
6. Ngan HY, Pang GK, Yung S, Ng MK. Wavelet based methods on patterned fabric defect detection. *Pattern Recognit*. 2005;38: 559-576.
7. Liu JJ, MacGregor JF. Estimation and monitoring of product aesthetics: application to manufacturing of "engineered stone" countertops. *Mach Vis Appl*. 2006;16:374-383.
8. Lin HD. Automated visual inspection of ripple defects using wavelet characteristic based multivariate statistical approach. *Image Vis Comput*. 2007;25:1785-1801.
9. Lin HD. Computer-aided visual inspection of surface defects in ceramic capacitor chips. *J Mater Process Technol*. 2007;189:19-25.
10. Lin HD, Chung CY, Lin WT. Principal component analysis based on wavelet characteristics applied to automated surface defect inspection. *WSEAS Trans Comput Res*. 2008;3:193-202.
11. Li WC, Tsai DM. Wavelet-based defect detection in solar wafer images with inhomogeneous texture. *Pattern Recognit*. 2012;45:742-756.
12. Jiang BC, Jiang S. Machine vision based inspection of oil seals. *J Manuf Syst*. 1998;17:159-166.
13. Lu CJ, Tsai DM. Automatic defect inspection for LCDs using singular value decomposition. *Int J Adv Manuf Technol*. 2005;25:53-61.
14. Tunák M, Linka A. Directional defects in fabrics. *Res J Text Appar*. 2008;12:13-22.
15. Armingol JM, Otamendi J, De La Escalera A, Pastor JM, Rodriguez FJ. Statistical pattern modeling in vision-based quality control systems. *J Intell Robot Syst*. 2003;37:321-336.
16. Jiang B, Wang CC, Liu HC. Liquid crystal display surface uniformity defect inspection using analysis of variance and exponentially weighted moving average techniques. *Int J Prod Res*. 2005;43:67-80.
17. Megahed FM, Woodall WH, Camelio JA. A review and perspective on control charting with image data. *J Qual Technol*. 2011;43:83-98.
18. Megahed FM, Wells LJ, Camelio JA, Woodall WH. A spatiotemporal method for the monitoring of image data. *Qual Reliab Eng Int*. 2012;28:967-980.
19. Chicken E. Block thresholding and wavelet estimation for nonequispaced samples. *J Stat Plann Infer*. 2003;116:113-129.
20. Nikoo M, Noorossana R. Phase II monitoring of nonlinear profile variance using wavelet. *Qual Reliab Eng Int*. 2013;29:1081-1089.
21. Chicken E, Pignatiello JJ Jr, Simpson JR. Statistical process monitoring of nonlinear profiles using wavelets. *J Qual Technol*. 2009;41:198-212.
22. Chicken E, Cai TT. Block thresholding for density estimation: local and global adaptivity. *J Multivar Anal*. 2005;95:76-106.
23. Jin J, Shi J. Automatic feature extraction of waveform signals for in-process diagnostic performance improvement. *J Intell Manuf*. 2001;12:257-268.
24. Vidakovic B. *Statistical Modeling by Wavelets*. Interscience John Wiley & Sons; 2009.
25. Daubechies I. *Ten Lectures on Wavelets*. Philadelphia, PA: SIAM; 1992.
26. Qiu P. *Image Processing and Jump Regression Analysis*. New York: John Wiley & Sons; 2005.
27. Reynolds MR Jr, Lou J. An evaluation of a GLR control chart for monitoring the process mean. *Journal of quality technology*. 2010;42:287–310.

Mehdi Koosha is a PhD candidate in Industrial Engineering at the Iran University of Science and Technology. He recieved his BS from faculty of Industrial Engineering of Islamic Azad University and his MS from Shahed Universiry. His research interests are statistical process monitoring and applied statistics.

Rassoul Noorossana is professor of Applied Statistics at Iran University of Science and Technology. He received his BS in engineering from Louisiana State University in 1983 and his MS and PhD in Engineering Management and Statistics from the University of Louisiana in 1986 and 1990, respectively. His primary research interests include statistical process control, process optimization, and data analysis. He is the editor of the Journal of Industrial Engineering International, associate editor of Quality Technology and Quantitative Management Journal, and serves on the editorial review board of many journals. He is a senior member of the American Society for Quality and Iranian Statistical Association.

Fadel Megahed is a professor in the Department of Information Systems and Analytics at Miami University. He recieved his PhD from the Grado Department of Industrial and Systems Engineering at Virginia Tech. He received his BS in Mechanical Engineering from the American University in Cairo and his MS in Industrial and Systems Engineering from Virginia Tech. His research interests include the application of statistical process control methodologies for image and laser scanning systems.

SUPPORTING INFORMATION

Supplementary documents including raw images of tiles, nominal image after pre-processing steps and simulation codes are available online (https://github.com/mehdikoosha/SPC-image-data-wavelets) to help readers and practitioners for replication of this work and making it easier for implementation in industries.

How to cite this article: Koosha M, Noorossana R, Megahed F. Statistical process monitoring via image data using wavelets. *Qual Reliab Engng Int*. 2017;33: 2059–2073. https://doi.org/10.1002/qre.2167